Experimental Cell Research 383 (2019) 111511

Contents lists available at ScienceDirect

Experimental Cell Research

journal homepage: www.elsevier.com/locate/yexcr

MSC-triggered metabolomic alterations in liver-resident immune cells isolated from CCl_4-induced mouse ALI model

Xiaowei Shi[a,b], Jingqi Liu[d,e], Deying Chen[c,e], Minglei Zhu[d], Jiong Yu[c,e], Haiyang Xie[a,b], Lin Zhou[a,b,c], Liang Li[c,d], Shusen Zheng[a,b,c,*]

[a] Division of Hepatobiliary and Pancreatic Surgery, Department of Surgery, The First Affiliated Hospital, School of Medicine, Zhejiang University, 79 Qingchun Rd., Hangzhou, 310003, China
[b] NHFPC Key Laboratory of Combined Multi-organ Transplantation, Hangzhou, 310003, China
[c] Collaborative Innovation Center for Diagnosis and Treatment of Infectious Diseases, 79 Qingchun Rd., Hangzhou, 310003, China
[d] Department of Chemistry, University of Alberta, Edmonton, Alberta, T6G 2G2, Canada
[e] State Key Laboratory for the Diagnosis and Treatment of Infectious Diseases, The First Affiliated Hospital, College of Medicine, Zhejiang University, 79 Qingchun Rd., Hangzhou, 310003, China

ARTICLE INFO

Keywords:
Mesenchymal stem cell
Liver-resident immune cells
Acute liver injury
Metabolomics
Chemical isotope labeling
Liquid chromatography – mass spectrometry
Pathway analysis

ABSTRACT

Clinical trials testing mesenchymal stem cell (MSC) as a cellular remedy for acute liver injury (ALI) are underway, but its underlying mechanism has not been thoroughly scrutinized. We highlight that the metabolomic profile of the liver-resident immune cells is significantly altered after MSC administration; its potential correlation with ALI remission is discussed in this study. C57BL/6 mice are randomly divided into three groups: the sham group, MSC-treated ALI group and PBS-treated ALI group; acute liver injury is induced by intraperitoneal injection of carbon tetrachloride. A high-performance chemical isotope labeling liquid chromatography–mass spectrometry (CIL LC–MS) is exploited to profile amine, phenol and carbonyl submetabolome of the liver-resident immune cells in different treatments. 4295 peak pairs are quantified and 2461 peak pairs are further identified in zero-reaction and one-reaction libraries. Clear separation of the three groups is observed in the global PCA and OPLS-DA analyses. We identified 256 metabolites to be candidate biomarkers for ALI-activated immunity and 114 metabolites to be candidate biomarkers for MSC-modulated immunity. Ariginine, aspartate and glutamate metabolism are most affected in both cases, with eight significantly regulated metabolites as joints (glutamic-gamma-semialdehyde, aspartate acid, glutamate acid, gamma-Aminobutyric acidorinithine, 2-keto-glutaramic acid, *N*-acetylornithine, citrulline and ornithine). These findings shed new light on the therapeutic benefit of immune modulation during ALI rescue. It needs to be further investigated whether exogenous supply of certain metabolites will exert a profound impact on the metabolic network, crosstalking with immune responses and modulating ALI prognosis.

1. Introduction

Acute liver injury (ALI) is a life-threatening condition where the rapid loss of hepatocytes subsequently leads to coagulopathy and encephalopath [1]. For the past few decades, limited options are available to manage ALI, such as liver support systems [2] that assist with detoxification and metabolic homeostasis, and liver transplantation. Recently, thorough comprehension of ALI pathology has brought forward novel strategies to compensate donor organ shortage in liver transplantation. Mechanisms for liver dysfunction can be classified into two categories: the direct damage from pathogens or toxic substances [3] and the indirect damage from immune-mediated inflammatory responses. Generally, innate and adaptive immune systems work synergistically in the recognition and clearance of pathogens and

Abbreviations: MSC, mesenchymal stem cell; ALI, acute liver injury; QC, Quality control; CIL LC – MS, chemical isotope labeling liquid chromatography – mass spectrometry; CCl_4, carbon tetrachloride; PCA, principal component analysis; OPLS-DA, orthogonal partial least squares discriminant analysis; DnsCl, dansylchloride; DnsHz, dansylhydrazine

* Corresponding author. Division of Hepatobiliary and Pancreatic Surgery, Department of Surgery, The First Affiliated Hospital, School of Medicine, Zhejiang University, 79 Qingchun Rd., Hangzhou, 310003, China.

E-mail addresses: xiaoweishi@zju.edu.cn (X. Shi), jqliu97@zju.edu.cn (J. Liu), deyingchen@zju.edu.cn (D. Chen), minglei@ualberta.ca (M. Zhu), yujiong@zju.edu.cn (J. Yu), xiehy@zju.edu.cn (H. Xie), zhoulin99@zju.edu.cn (L. Zhou), liang.li@ualberta.ca (L. Li), shusenzheng@zju.edu.cn (S. Zheng).

https://doi.org/10.1016/j.yexcr.2019.111511
Received 27 April 2019; Received in revised form 4 July 2019; Accepted 24 July 2019
Available online 27 July 2019
0014-4827/

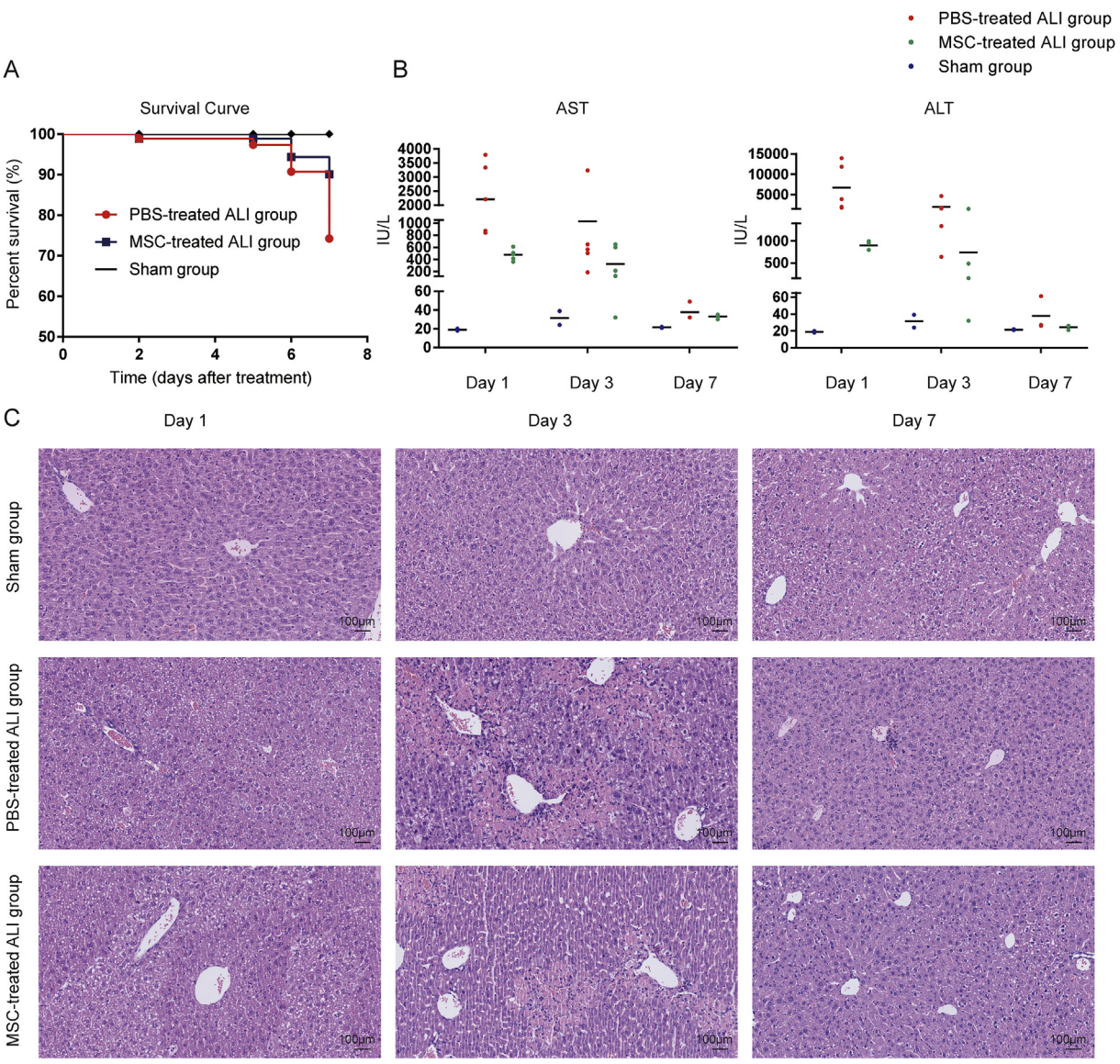

Fig. 1. Mesenchymal stem cells (MSCs) therapy attenuates acute liver injury. Samples are collected on day 1, day 3 and day 7 after carbon tetrachloride (CCl_4) administration or sham operation. (A) Kaplan-Meier plot for mouse survival after CCl_4 administration (1.5 mL/kg) or sham operation. MSC or PBS injection is performed 6 h later. N = 22 per group. (B) Liver aspartate aminotransferase (AST) and alanine aminotransferase (ALT) levels of PBS-treated ALI group, MSC-treated ALI group and the sham group. (C) Hematoxylin and eosin staining of mouse livers.

impaired tissues. However, in the case of ALI, immune responses become a double-edged sword for the host, for example, overproduction of cytokines, if unchecked, contributes to ALI via inordinate liver cell death and causes severe outcomes [4].

As supported by growing evidence, mesenchymal stem cell (MSC) is a promising cure for liver diseases [5]. MSCs were first isolated from the bone marrow and later from a variety of tissues as cells capable of multipotent differentiation. The relative ease of harvesting MSCs, and their stable phenotype under *in vitro* culture, make them an attractive tool for cellular therapy [6]. MSC therapy may also serve as an ideal alternative for ALI treatment [7,8], as the immune-regulatory [9] and regenerative properties of MSCs mitigate the overreaction of immune system and promote hepatocyte regeneration.

There is interest in fully elucidating how immunity responds to MSC rescue and how this response contributes to ALI amelioration. Our previous study revealed inhibited proliferation of conventional natural killer (cNK) cells, plasma dendritic cells (pDCs), $CD4^+$ T cells, γδ T cells, and B cells and induced proliferation of monocytes, monocyte-derived macrophages, myeloid-derived suppressor cell (MDSC)-like cells and Tregs are observed in MSC-treated ALI with improved liver restitution.

Metabolomics studies allow us to discover metabolites involved in disease mechanisms by monitoring metabolite level changes [10]. Certain metabolites or metabolic patterns have been proved to be valid indicators for immune modulations. For example, the Warburg effect is a hallmark of inflammatory cells, whereas a shift towards oxidative phosphorylation is indicative of anti-inflammatory cells [11]. Metabolomic methodology has emerged and offers a powerful tool to further explore the interplay between metabolism and immune responses. Metabolic profiling of immune cells is able to provide a functional readout of their physiological changes after MSC administration.

In this study, a high-performance chemical isotope labeling liquid chromatography–mass spectrometry (CIL LC–MS) is introduced to systematically analyze the metabolic profile of the liver-resident immune cells in carbon tetrachloride (CCl_4)-induced murine acute liver injury (ALI) model. Combining a sample normalization strategy and differential isotope labeling, CIL LC–MS aims to improve detection sensitivity, metabolomic coverage, quantification precision and

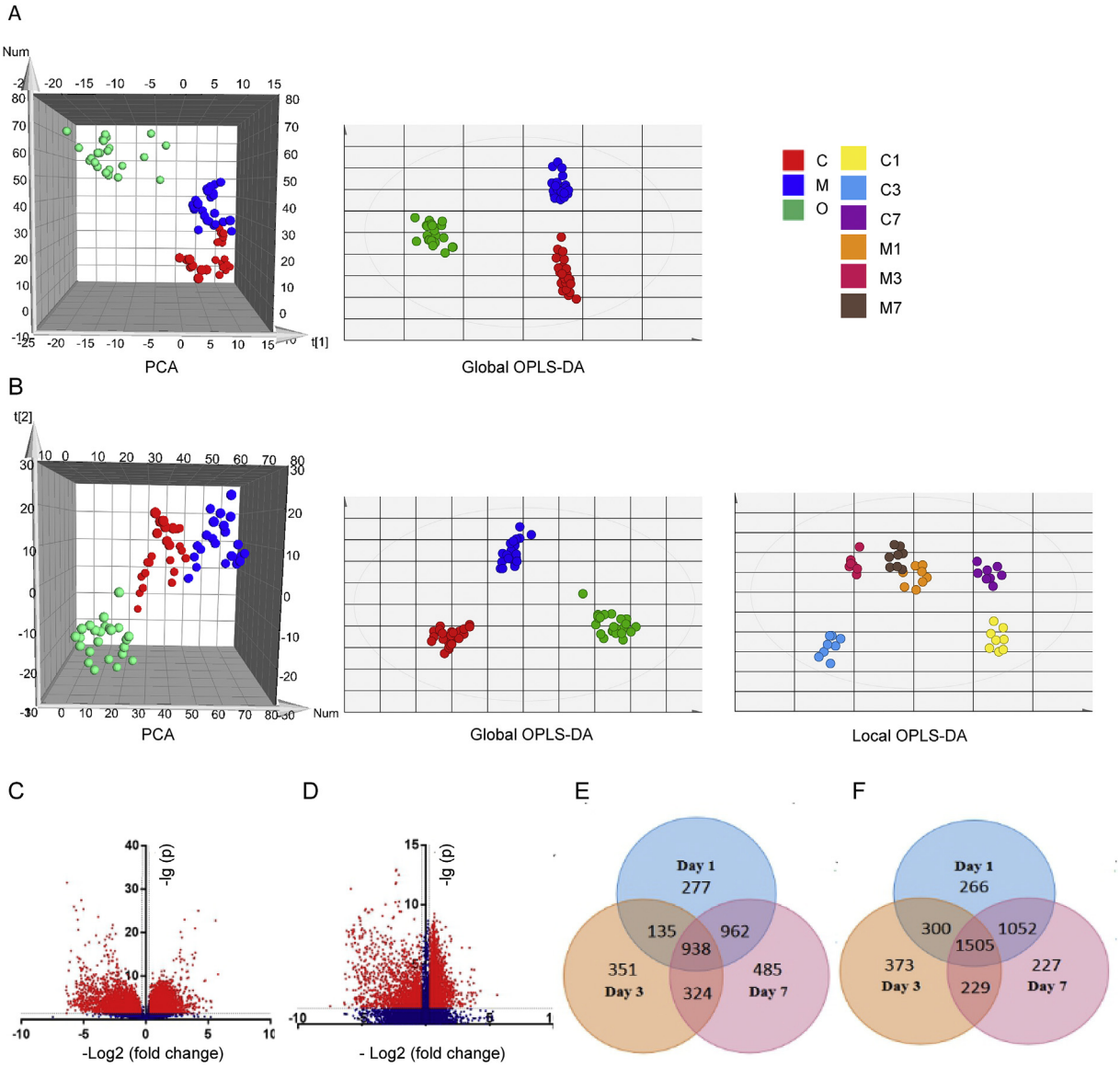

Fig. 2. Comprehensive analyses of metabolomic data. Principal component analysis (PCA) score plots and orthogonal partial least squares discriminant analysis (OPLS-DA) score plots for the (A) dansylchloride and (B) dansylhydrazine labeled metabolomic profiles of the liver-resident immune cells that are collected from different treatments. (C) Volcano plots for peak pairs that significantly vary from PBS-treated ALI to the sham group at three time points. (D) Volcano plots for peak pairs that significantly vary from MSC-treated ALI to PBS-treated ALI at three time points. The variation is considered to be significant if fold change ≥ 1.2, and *p-value* < 0.05. Samples are collected on day 1, day 3, and day 7 after CCl_4 administration or sham operation. (E) Venn diagram presenting the numbers of peak pairs that significantly varied from MSC-treated ALI to the PBS-treated ALI at three time points. (F) Venn diagram presenting the numbers of peak pairs that significantly varied from PBS-treated ALI to the sham group at three time points.

quantification accuracy [12]. By digging into metabolomic profiles of the sham group, PBS-treated ALI and MSC-treated ALI group, we aim to: (1) prove that MSC administration is beneficial for ALI remission; (2) quantify MSC-triggered metabolomic alterations in liver-resident immune cells during ALI progression; (3) pick out potential biomarkers or mediators for immune modulation; (5) cast new light on the correlation between ALI remission and metabolic perturbations within liver-resident immune cells after MSC rescue.

2. Methods

2.1. Isolation, culture and identification of MSCs

All experimental procedures are conducted according to a protocol approved by the Ethics Committee of the First Affiliated Hospital, School of Medicine, Zhejiang University (Reference number: 2015-130). All mouses were housed in an air-conditioned animal room with 50% humidity and a 12-h daylight/darkness cycle in Experimental Animal Center of Zhejiang University.

Inbred 2-week-old green fluorescent protein (GFP) transgenic mice (male and female, C57BL/6 background) are purchased from Nanjing Biomedical Research Institute of Nanjing University, Nanjing, China. A previous protocol [13] is applied to isolate MSCs from compact bone. Isolated MSCs are cultured in complete media (OriCell™C57BL/6 MSC complete medium; Cyagen Biosciences, Guangzhou, China) at 37 °C, 5% CO_2 incubator (HERA cell®150; Thermo Fisher Scientific Inc., Waltham, MA, USA). Phenotype examination, osteogenic and adipogenic differentiation are performed to confirm the multipotency of MSCs from passage 3 and 5 that are used throughout the experiments.

Table 1
Metabolites that are shared in the two groups of candidate biomarkers.

Query	Hit
HMDB01439	Phosphoribosyl formamidocarboxamide
HMDB01149	5-Aminolevulinic acid
HMDB02104	L-Glutamic gamma-semialdehyde
HMDB06272	5-Amino-2-oxopentanoic acid
HMDB01080	4-Aminobutyraldehyde
HMDB12135	1-(3-Aminopropyl)-4-aminobutanal
HMDB01240	Pseudooxynicotine
HMDB12246	Kynuramine
HMDB12149	2-Isopropyl-3-oxosuccinate
HMDB11714	Vanilpyruvic acid
HMDB01252	Betaine aldehyde
HMDB06293	L-Erythrulose
HMDB04181	Methylimidazole acetaldehyde
HMDB11683	Molybdopterin precursor Z
HMDB03312	Daidzein
HMDB11639	Topaquinone
HMDB06833	2-Acetolactate
HMDB06855	(S)-2-Acetolactate
HMDB04083	4-(2-Amino-3-hydroxyphenyl)-2,4-dioxobutanoic acid
HMDB11718	4-Hydroxybenzaldehyde
HMDB06115	Benzaldehyde
HMDB00978	4-(2-Aminophenyl)-2,4-dioxobutanoic acid
HMDB01430	L-Dopachrome
HMDB04086	5-Hydroxy-*N*-formylkynurenine
HMDB00715	Kynurenic acid

2.2. CCl_4-induced murine acute liver failure model and MSC treatment

Eight-week-old male wild-type C57BL/6 mice (weight, 20–25 g) are purchased from Shanghai SLAC Laboratory Animal CoLtd., Shanghai, China. A mixture of carbon tetrachloride (Sigma-Aldrich, St. Louis, MO, USA)/olive oil (Sigma-Aldrich) (CCl_4/olive oil, 1:1, v/v) is prepared and is later injected intraperitoneally with a dose of 3 ml/kg body weight to induce acute liver injury (ALI). The sham group receives an intraperitoneal injection of pure olive oil (Sigma-Aldrich) with the same dose. 100 μl of phosphate-buffered saline (PBS) with or without 5×10^5 MSCs is injected into MSC-treated ALI and PBS-treated ALI group via caudal vein 6 h after CCl_4 administration, respectively.

2.3. Liver biochemistry and liver histology

For histopathologic analysis, formalin-fixed liver samples are paraffin-embedded, sectioned (5 μl thickness), and stained with hematoxylin and eosin. The sections are randomly numbered prior to evaluation by an experienced pathologist. Images are generated by NanoZoomer 2.0-RS scanner (Hamamatsu Photonics KK, Hamamatsu City, Japan) equipped with scanner software. Alanine aminotransferase (ALT) and aspartate aminotransferase (AST) activities of serum samples are measured using a dry chemistry analyzer (FUJI DRI-CHEM 4000ie; Fujifilm Corporation, Tokyo, Japan).

2.4. Isolation of immune cells

Murine liver is first perfused with PBS for blood removal and then digested by a Mouse Liver Dissociation Kit (Miltenyi Biotec, Bergisch Gladbach, Germany) following the manufacturer's instructions. The homogenate is centrifuged (Thermo Scientific, Waltham, MA, USA) at 300 g for 10 min to remove supernatant and harvest the non-parenchymal cells. The cells are further confirmed to be immune cells with CD45 (30-F11; BioLegend®, Enabling Legendary Discovery®, San Diego, USA) surface marker by flow cytometry (BeamCyte-1026, Beamdiag, Changzhou, China).

2.5. Metabolite extraction

Metabolite extraction is prepared following a previous procedure by Luo and Lorenz [14,15] with some modification.

Isolated immune cells are quenched in 1 ml of methanol/water mixture ($MeOH/H_2O$, 1:1, v/v, −20 °C, Fisher Chemical, Waltham, MA, USA). Cell suspension is transferred into a 1.5 ml centrifuge tube (Thermo Scientific) and then centrifuged at 12000 rpm, 4 °C for 4 min (Beckman Coulter Microfuge 22R centrifuge, Brea, CA, USA). 900 μl of supernatant is put aside into a new tube. 0.5 ml of 1.0-mm-diameter glass beads (Biospec Products, USA) is added to cell sediment. Five repeats of 1 min bead–beating at 2500 rpm on a Touch Mixer Model 232 (Fisher Scientific, USA) followed by 1 min ice bath are performed for cell lysis. Lysed cells are resuspended in the former supernatant, and are centrifuged at 12000 rpm, 4 °C for 5 min to remove cell debris. The supernatant is transferred to a new vial and dried in a refrigerated CentriVap concentrator system (Labconco, Kansas City, MO, USA). Dried metabolite extracts are stored at −80 °C.

2.6. Isotope labeling reaction and LC-MS

^{12}C-dansylchloride (light chain) is purchased from Sigma-Aldrich (St. Louis, MO) and ^{13}C-dansylchloride (heavy chain) is synthesized in house as previously described by Prof. Liang Li (mcid.chem.-ualberta.ca). Dansylhydrazine (DnsHz) is prepared by treating dansylchloride with hydrazine following a literature procedure with some modification [16,17].

The dried metabolites are redissolved in 100 μL of water (LC-MS grade, Sigma-Aldrich). 20 μL of solution of the individual sample is used for ^{12}C-DnsCl, ^{13}C-DnsCl, ^{12}C-DnsHz and ^{13}C-DnsHz labeling, respectively.

For dansylchloride labeling, 20 μL of sample solution is mixed with 20 μL of sodium carbonate/sodium bicarbonate buffer (0.5 mol/L, pH 9.4). 20 μL of 20 mM ^{12}C-DnsCl or ^{13}C-DnsCl is added after vortexing and spinning down the sample solution and the mixture is then incubated at 60 °C, 150 rpm for 60 min on a shaker (Innova-4000 benchtop incubator shaker). After incubation, solutions are vortexed, spun down and added with 30 μL of 0.5 M methylamine to remove redundant dansylchloride. The mixtures are again vortexed and spun down, and incubated at 60 °C for another 30 min [18].

For dansylhydrazine labeling, 20 μL of sample solution is mixed with 20 μL of 144 mM HCl solution and 20 μL of 20 mM ^{12}C-DnsHz or ^{13}C-DnsHz. The mixture is first vortexed and spun down and then incubated at 40 °C for 60 min. Acid catalyst is removed from the cooled mixture by SpeedVac (Thermo Scientific). 80 μL of acetonitrile/water mixture (ACN/H_2O, 50:50, v/v) is used to redissolve the dried metabolites [12].

The ^{12}C-/^{13}C-DnsCl and ^{12}C-/^{13}C-DnsHz mixture is diluted and centrifuged at 15294 g for 10 min before LC-MS for analysis. The quality control (QC) sample was a 1:1 mixture of ^{12}C-labeled and ^{13}C-labeled pool and QC sample was injected every 10 sample runs as the critical requirement for acceptable normalization.

2.7. Data processing and analysis

CIL LC-MS data are processed by a series of software programs that are previously developed in house [19]. First, peak pairs with only a protonated ion are retained after redundant pair filtration (e.g., those of adduct ions and dimers) by IsoMS. The intensity ratio calculation and multiple-pair-alignment of retained peak pairs are performed according to retention time and accurate mass.

Second, a Zerofill program [20] is used to fill in the missing values of the intensity ratios mentioned above.

Then, the final metabolite-intensity table for relative quantification is generated by IsoMS-Quant [21], which determines the chromatographic peak ratio of each peak pair. Certain metabolites are selected as

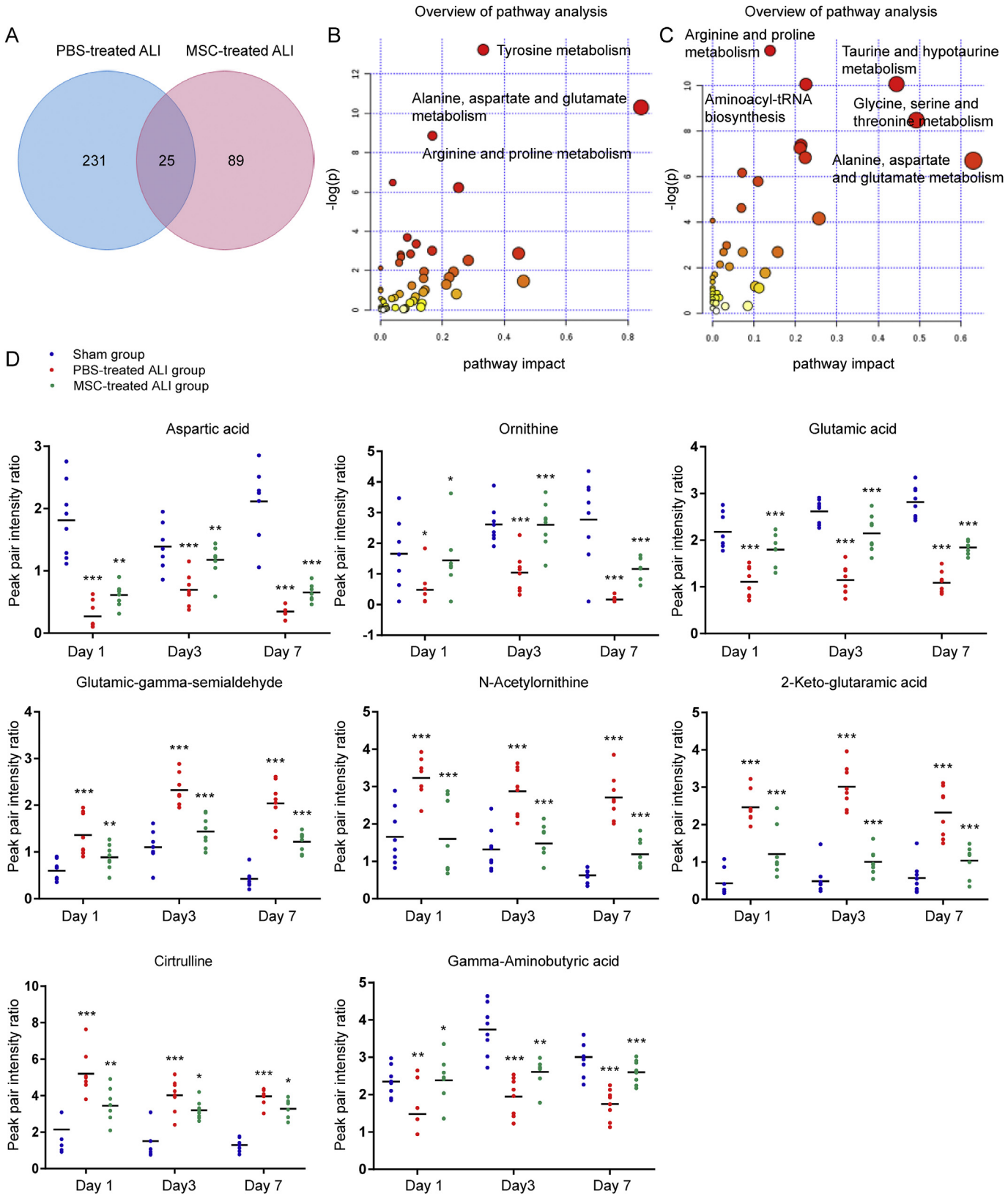

Fig. 3. Potential biomarkers for ALI-activated and MSC-modulated immune responses and overview graphs for metabolic pathway analysis. (A) A Venn diagram presenting the numbers of identified metabolites that are significantly regulated after ALI activation or MSC treatment. (B) Overview of pathways based on metabolites that significantly vary from PBS-treated ALI to the sham group continuously on three time points (day 1, day 3, and day 7 after CCl_4 administration or sham operation). (C) Overview of pathways based on metabolites that significantly vary from MSC-treated ALI to PBS-treated ALI continuously on three time points. Pathways with smaller p-values and greater pathway impact value are considered to be most affected. (D) Peak pair intensity ratios of eight metabolites are presented as independent data points. Paired student's t-test is performed to analyze intensity alterations in PBS-treated ALI versus the sham group and PBS-treated ALI versus MSC-treated ALI. Samples are collected on day 1, day 3, and day 7 after CCl_4 administration or sham operation. *$p < 0.05$, **$p < 0.01$, ***$p < 0.001$.

Table 2
Metabolic pathway analysis for candidate biomarkers during acute liver injury-related immunity.

Pathway Name	Match Status	*p*	-log(p)	Holm p	FDR	Impact
Tyrosine metabolism	19/76	1.7868E-6	13.235	1.4295E-4	1.4295E-4	0.33193
Alanine, aspartate and glutamate metabolism	9/24	3.3586E-5	10.301	0.0026533	0.0013434	0.84236
Arginine and proline metabolism	16/77	1.4216E-4	8.8585	0.011089	0.003791	0.16761
Phenylalanine metabolism	10/45	0.0015369	6.478	0.11835	0.030739	0.03926
Tryptophan metabolism	14/79	0.0019886	6.2203	0.15113	0.031818	0.25205
Nitrogen metabolism	7/39	0.025035	3.6875	1.0	0.3338	0.08613
Pyrimidine metabolism	9/60	0.034795	3.3583	1.0	0.39766	0.11511
Pantothenate and CoA biosynthesis	5/27	0.049218	3.0115	1.0	0.43543	0.16654
beta-Alanine metabolism	5/28	0.056367	2.8759	1.0	0.43543	0.44629
Cysteine and methionine metabolism	8/56	0.058065	2.8462	1.0	0.43543	0.09697
Taurine and hypotaurine metabolism	4/20	0.059871	2.8156	1.0	0.43543	0.06474
Glycine, serine and threonine metabolism	7/48	0.067492	2.6957	1.0	0.44995	0.06612
Selenoamino acid metabolism	4/22	0.08038	2.521	1.0	0.49464	0.28353
Lysine biosynthesis	5/32	0.090595	2.4014	1.0	0.51768	0.05973
D-Arginine and D-ornithine metabolism	2/8	0.11884	2.1299	1.0	0.63383	0.0
Lysine degradation	6/47	0.14233	1.9496	1.0	0.67895	0.14045
Valine, leucine and isoleucine biosynthesis	4/27	0.14428	1.936	1.0	0.67895	0.23583
Citrate cycle (TCA cycle)	3/20	0.19068	1.6572	1.0	0.84745	0.22169
D-Glutamine and D-glutamate metabolism	2/11	0.20149	1.602	1.0	0.84837	0.13904
Retinol metabolism	3/22	0.23143	1.4635	1.0	0.92573	0.46186
Propanoate metabolism	4/35	0.2735	1.2964	1.0	1.0	0.21243
Ubiquinone and other terpenoid-quinone biosynthesis	4/36	0.29102	1.2344	1.0	1.0	0.10099
Cyanoamino acid metabolism	2/16	0.34647	1.0599	1.0	1.0	0.0
Butanoate metabolism	4/40	0.36217	1.0157	1.0	1.0	0.14355
Synthesis and degradation of ketone bodies	1/6	0.37809	0.97263	1.0	1.0	0.0
Sulfur metabolism	2/18	0.40267	0.90963	1.0	1.0	0.13819
Glycerolipid metabolism	3/32	0.44392	0.8121	1.0	1.0	0.0618
Pyruvate metabolism	3/32	0.44392	0.8121	1.0	1.0	0.24509
Aminoacyl-tRNA biosynthesis	6/75	0.51176	0.66989	1.0	1.0	0.11268
Glyoxylate and dicarboxylate metabolism	4/50	0.53492	0.62563	1.0	1.0	0.04601
Thiamine metabolism	2/24	0.55522	0.58839	1.0	1.0	0.0
Glutathione metabolism	3/38	0.56125	0.57759	1.0	1.0	0.03571
Phenylalanine, tyrosine and tryptophan biosynthesis	2/27	0.62056	0.47713	1.0	1.0	0.00738
Steroid hormone biosynthesis	7/99	0.63806	0.44933	1.0	1.0	0.10571
Histidine metabolism	3/44	0.66246	0.41179	1.0	1.0	0.00912
Glycolysis or Gluconeogenesis	2/31	0.69589	0.36256	1.0	1.0	0.0953
Purine metabolism	6/92	0.71363	0.33739	1.0	1.0	0.13382
Valine, leucine and isoleucine degradation	2/40	0.82088	0.19737	1.0	1.0	0.01657
Nicotinate and nicotinamide metabolism	2/44	0.86001	0.15081	1.0	1.0	0.0
Ascorbate and aldarate metabolism	2/45	0.86849	0.141	1.0	1.0	0.13047
Fructose and mannose metabolism	2/48	0.8912	0.11519	1.0	1.0	0.04741
Pentose and glucuronate interconversions	2/53	0.92116	0.082125	1.0	1.0	0.08036
Pentose phosphate pathway	1/32	0.92172	0.081513	1.0	1.0	0.0
Vitamin B6 metabolism	1/32	0.92172	0.081513	1.0	1.0	0.01914
Terpenoid backbone biosynthesis	1/33	0.92775	0.07499	1.0	1.0	0.0
Methane metabolism	1/34	0.93332	0.069005	1.0	1.0	0.01696
Limonene and pinene degradation	2/59	0.9469	0.054559	1.0	1.0	0.07672
Inositol phosphate metabolism	1/39	0.95538	0.04565	1.0	1.0	0.01203
Glycerophospholipid metabolism	1/39	0.95538	0.04565	1.0	1.0	0.07378
Arachidonic acid metabolism	1/62	0.99305	0.0069786	1.0	1.0	0.0
Metabolism of xenobiotics by cytochrome P450	1/65	0.99455	0.0054643	1.0	1.0	0.0
Porphyrin and chlorophyll metabolism	2/104	0.99779	0.0022174	1.0	1.0	0.00815

candidate biomarkers for ALI progression and immunomodulation after fold-change and paired Student's t-test analyses.

Selected metabolites are matched and identified in zero-reaction and one-reaction libraries [22] that are now freely available on www.mycompoundid.org Finally, an overview of the affected pathways based on selected metabolites is presented by MetaboAnalyst 3.0.

3. Results

3.1. MSCs therapy attenuates acute liver injury

MSC morphology, phenotype, osteogenic and adipogenic differentiation are confirmed prior to administration. Cells exhibit adherence dependency, fibroblast-like morphology (Supplementary Fig. S1A) and the ability to differentiate into adipocytes and osteoblasts (Supplementary Figs. S1B and S1C). Flow cytometry verifies that cells express CD44, CD29, and Sca-1 but not CD31, CD45, CD11b, CD86 or MHC II (Supplementary Fig. S1D), consistent with immunophenotypic characteristics of typical mesenchymal lineages.

The mortality rate, liver histology and liver function parameters are assessed in the sham group, PBS-treated ALI and MSC-treated ALI group that are sacrificed on day 1, day 3 and day 7 after CCl_4 administration or sham operation, respectively. As ALI develops, death occurs 2 days after CCl_4 administration. MSC-treated ALI presents a considerable lower mortality rate compared to PBS-treated ALI (18% vs. 45.5%) 7 days after CCl_4 administration (Fig. 1A).

Impaired liver function is revealed by elevated alanine aminotransferase (ALT) and aspartate aminotransferase (AST) level, which peaks 1 day after CCl_4 administration and gradually restores 7 days after CCl_4 administration in PBS-treated ALI and MSC-treated ALI. Considerably reduced level of ALT and AST in MSC-treated ALI suggests attenuated liver dysfunction (Fig. 1B).

Sequential histopathological features of ALI are observed at indicated time points, ranging from hepatocyte hydropic degeneration,

Table 3
Metabolic pathway analysis for candidate biomarkers during immune modulation after mesenchymal stem cells treatment.

Pathway Name	Match Status	*p*	-log(p)	Holm p	FDR	Impact
Purine metabolism	17/92	3.4272E-7	14.886	2.7417E-5	2.7417E-5	0.20074
Arginine and proline metabolism	12/77	1.2471E-4	8.9895	0.0098523	0.0049885	0.21733
Glycine, serine and threonine metabolism	9/48	2.188E-4	8.4273	0.017067	0.0058348	0.2782
Valine, leucine and isoleucine biosynthesis	5/27	0.0063098	5.0656	0.48586	0.1262	0.16535
Tyrosine metabolism	8/76	0.019747	3.9248	1.0	0.31595	0.04517
Sulfur metabolism	3/18	0.04489	3.1035	1.0	0.50897	0.00157
D-Arginine and D-ornithine metabolism	2/8	0.047587	3.0452	1.0	0.50897	0.0
Lysine biosynthesis	4/32	0.053893	2.9208	1.0	0.50897	0.14524
Lysine degradation	5/47	0.058698	2.8354	1.0	0.50897	0.12809
Tryptophan metabolism	7/79	0.063622	2.7548	1.0	0.50897	0.19003
Glutathione metabolism	4/38	0.090183	2.4059	1.0	0.60481	0.05854
Valine, leucine and isoleucine degradation	4/40	0.10435	2.26	1.0	0.60481	0.03378
Cysteine and methionine metabolism	5/56	0.10658	2.2389	1.0	0.60481	0.07718
Pantothenate and CoA biosynthesis	3/27	0.12039	2.1171	1.0	0.60481	0.02055
Phenylalanine, tyrosine and tryptophan biosynthesis	3/27	0.12039	2.1171	1.0	0.60481	0.0738
Aminoacyl-tRNA biosynthesis	6/75	0.12096	2.1123	1.0	0.60481	0.05634
Taurine and hypotaurine metabolism	2/20	0.2285	1.4762	1.0	1.0	0.08093
Nitrogen metabolism	3/39	0.25817	1.3541	1.0	1.0	0.09151
Fructose and mannose metabolism	3/48	0.37161	0.9899	1.0	1.0	0.04214
Biotin metabolism	1/11	0.40001	0.91626	1.0	1.0	0.07317
Vitamin B6 metabolism	2/32	0.42947	0.8452	1.0	1.0	0.17727
Pyrimidine metabolism	3/60	0.51672	0.66025	1.0	1.0	0.03548
Cyanoamino acid metabolism	1/16	0.52472	0.64489	1.0	1.0	0.0
Histidine metabolism	2/44	0.60064	0.50975	1.0	1.0	0.00861
Riboflavin metabolism	1/21	0.62369	0.4721	1.0	1.0	0.10178
Selenoamino acid metabolism	1/22	0.64088	0.44491	1.0	1.0	0.08193
Alanine, aspartate and glutamate metabolism	1/24	0.67296	0.39606	1.0	1.0	0.02374
Sphingolipid metabolism	1/25	0.68792	0.37408	1.0	1.0	0.0
beta-Alanine metabolism	1/28	0.72885	0.31629	1.0	1.0	0.02328
Amino sugar and nucleotide sugar metabolism	3/88	0.77184	0.25898	1.0	1.0	0.01344
Pyruvate metabolism	1/32	0.77526	0.25456	1.0	1.0	0.0
Methane metabolism	1/34	0.79542	0.22889	1.0	1.0	0.01751
Propanoate metabolism	1/35	0.80482	0.21714	1.0	1.0	0.0
Ubiquinone and other terpenoid-quinone biosynthesis	1/36	0.81378	0.20606	1.0	1.0	0.0
Butanoate metabolism	1/40	0.84576	0.16752	1.0	1.0	0.04772
Folate biosynthesis	1/42	0.85964	0.15124	1.0	1.0	0.03372
Starch and sucrose metabolism	1/50	0.90382	0.10112	1.0	1.0	0.00137
Porphyrin and chlorophyll metabolism	1/104	0.99276	0.007265	1.0	1.0	0.00815

sinusoidal congestion to diffuse hepatic necrosis. Liver tissues show less necrosis on day 1 and day 3 and recover quickly on day 7 in MSC-treated ALI, while slight edema and individual necrotic cells can still be observed on day 7 in PBS-treated ALI (Fig. 1C).

In addition, GFP^+ MSCs are continuously detected within liver parenchymal cell suspension (Supplementary Fig. S1E-G) but absent from lungs, hearts, kidney, spleen, blood or lymph nodes, indicating successful and organ-specific settlement of MSCs.

3.2. Quantitative metabolomics of liver-resident $CD45^+$ immune cells

Flow cytometry verifies that cells isolated from the liver express CD45 surface marker (Supplementary Fig. S2). CIL LC-MS analyses are carried out following a workflow presented in graphic abstract (Supplementary Fig. S3). Dansylchloride (DnsCl) and dansylhydrazine (DnsHz) labeling are both applied to detect metabolites containing primary amine, secondary amine, phenolic hydroxyl groups, and various forms of carbonyl groups such as ketones and aldehydes, respectively. Sample normalization is performed to eliminate concentration variations among individual samples before quantitative metabolomic analyses. 1535 and 2760 peak pairs are quantified separately from ^{12}C-/^{13}C-isotope DnsCl labeling and DnsHz labeling (Supplementary Table S1A-B). The above results also illustrate that CIL LC-MS with DnsCl and DnsHz labeling is a promising tool for high-performance metabolomic analyses.

3.3. Comprehensive analyses of metabolomic data

3.3.1. PCA and PLS-DA analyses

Principal component analyses (PCA) and orthogonal partial least squares discriminant analyses (OPLS-DA) are performed in the first place to identify outliers and clusters within the sample population. The PCA and OPLS-DA score plots are displayed (Fig. 2A–B). Tight cluster of quality control (QC) samples assures instrument robustness throughout CIL LC–MS.

As for DnsCl-labeled metabolome, the sham group, MSC-treated ALI and PBS-treated ALI at all time points are separated in the global PCA plot. Sham group tends to cluster to the left part, while locations of ALI groups generally move to right and are further vertically separated by MSCs injection. The global OPLS-DA model also shows a clear separation of the three groups.

As for DnsHz-labeled metabolome, in the global OPLS-DA plot, dots of the sham group, MSC-treated ALI and PBS- treated ALI group converge to lower right area, upper median area and lower left area, respectively. Also, samples taken at different time points can be further separated in the local OPLS-DA plot (after removing the sham group from the plot). Clear separation of the three groups is observed in global PCA model.

3.3.2. Significance analyses for metabolomic data

Six pairwise comparisons (MSC-treated ALI versus PBS-treated ALI and PBS-treated ALI versus the sham group on day 1, day 3 and day 7 after CCl_4 administration or sham operation, respectively) are performed to investigate metabolomic variations. Peak pair intensity is considered to be significantly altered if average fold change ≥ 1.2 and

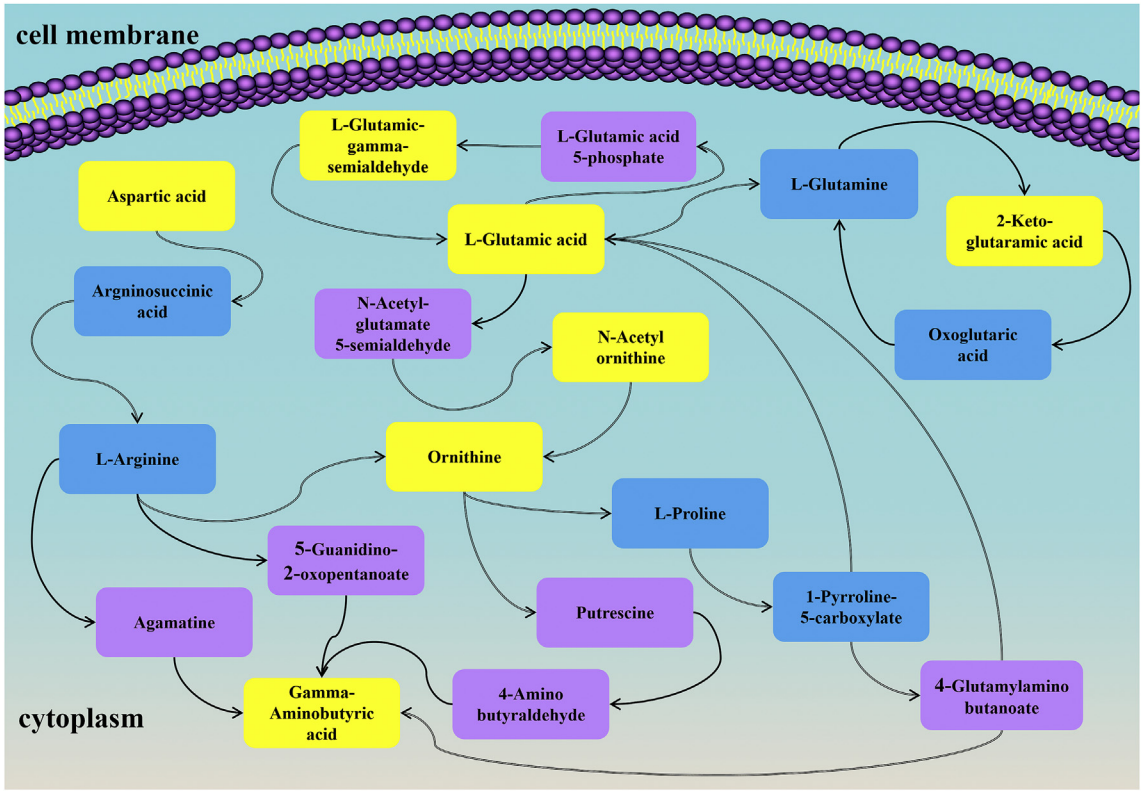

Fig. 4. Schematic illustration of arginine, aspartate and glutamate metabolism in cytoplasm. These three pathways are most affected in both PBS-treated ALI vs. sham group and MSC-treated ALI vs. PBS-treated ALI. Eight metabolites are commonly shared and significantly regulated by these pathways and are presented in yellow boxes. These metabolites are closely related to each other: L-aspartic acid is positioned upstream of arginine synthesis; reciprocal conversion among ornithine, glutamic-gamma-semialdehyde and *N*-acetylornithine associates arginine metabolism with glutamate metabolism; in addition, gamma-aminobutyric acid can be generated as a final product from both arginine and glutamate metabolism. Undetected metabolites are presented in blue boxes. Violet boxes represent other detected intermediates within each pathway.

p-value < *0.05*.

In total, significant alterations of 3952 peak pairs are detected in PBS-treated ALI versus the sham group and 3472 peak pairs are detected in MSC-treated ALI versus PBS-treated ALI, as presented in volcano plots (Fig. 2C–D). Detailed information about peak pair alterations on day 1, day 3 and day 7 are presented in Venn diagram (Fig. 2E–F).

3.4. Metabolites identification and biomarker selection

791 out of 1535 peak pairs (51.53%) in DnsCl labeling and 1671 out of 2760 peak pairs (60.54%) in DnsHz labeling are further identified in zero-reaction and one-reaction libraries (Supplementary Table S2A-B).

In this study, a criterion is exploited to uncover candidate biomarkers or mediators for immune responses during ALI. Metabolites that display continuously changing behaviors in different treatments can be interpreted as a reflection of varying immune status correlated with ALI progression or MSC immunomodulation. More specifically, metabolites that exhibit significant changes among PBS-treated ALI versus the sham group may play a crucial role in immune responses during ALI progression. On the other hand, oscillation of certain metabolites within MSC-treated ALI versus PBS-treated ALI may be closely related to immune modulation after MSC treatment. We identify 256 metabolites that exhibit significant concentration changes between PBS-treated ALI and the sham group at three time points and 114 metabolites exhibit oscillations within MSC-treated ALI and PBS-treated ALI at three time points. It's worth mentioning that some peak pairs have multiple matches in zero-reaction and one-reaction libraries, so the list of potential biomarkers could be refined by further comparison with standard samples.

Furthermore, there is an overlap of 25 metabolites (Table 1) between the two groups of candidate biomarkers mentioned above, as shown in Venn diagram (Fig. 3A). Since these 25 metabolites are key components of the featured metabolomic profile of liver-resident immune cells during ALI progression, and can be further modulated by MSC treatment, the perturbation of them may be an underlying mechanism for MSC-modulated immune responses and partially accounts for MSC-facilitated recovery in ALI.

3.5. Pathway analysis

Pathway analyses combining *p*-values (from pathway enrichment analysis) and pathway impact values (from pathway topology analysis) are performed to find out pathways that are greatly influenced by ALI-related or MSC-triggered metabolite perturbations. Overviews of the pathways related to candidate biomarkers are generated by Metaboanalyst 3.0. A summary of metabolic pathway analyses results are presented in Tables 2 and 3. Three pathways vary significantly from PBS-treated ALI to the sham group (Fig. 3B). Thirteen pathways exhibit a significant variation between MSC-treated ALI and PBS-treated ALI (Fig. 3C). Among them, five pathways including (1) arginine and proline metabolism, (2) taurine and hypotaurine metabolism, (3) aminoacyl-tRNA biosynthesis, (4) glycine, serine and threonine metabolism are most affected (with smaller *p*-values and greater pathway impact value) after MSC administration.

4. Discussion

Clinical trials testing MSC as a cellular remedy for liver diseases are underway [23], including acute liver injury (ALI), where the rapid loss of hepatocytes exceeds liver's regenerative capacity. There is interest in

fully elucidating the pathogenesis of these diseases and the underlying mechanisms for MSC rescue. New evidence suggests that ALI can be promoted by unchecked immune responses [4]. We speculate that MSCs trigger metabolic shifts in liver-resident immune cells as a robust approach for immune modulation and ALI rescue. In this work, we have employed CIL LC-MS to quantify metabolomic variations in the liver-resident immune cells from PBS-treated ALI, MSC-treated ALI and the sham group.

After CCl_4 administration, liver-resident immune cells rapidly distinguish damaged tissues and initiate inflammatory responses, during which they undergo a metabolic shift from quiescent to activated state, reallocating nutrients into different pathways to support functional changes. PLS-DA and OPLS-DA analyses are performed to evaluate the overall metabolomic distinctions among PBS-treated ALI, MSC-treated ALI and the sham group. Amine, phenol and carbonyl submetabolome are found to show interesting clusters associated with MSC treatment and ALI progression. Samples taken at different time points can be further separated in local OPLS-DA model, indicating that immune cells in each subgroup commit to a featured metabolic pattern as ALI develops.

Six pairwise comparisons (MSC-treated ALI versus PBS-treated ALI and PBS-treated ALI versus sham on day 1, day 3 and day 7 after CCl_4 administration or sham operation) are performed to identify metabolites with significantly altered concentrations. Continuously changing behaviors of the metabolic profile in different treatments can be viewed as a snapshot of varying immune status during ALI progression or MSC immunomodulation. 256 metabolites that exhibit significant concentration changes between PBS-treated ALI and the sham group at three time points are potential biomarkers for ALI-related immunity. On the other hand, oscillations of 114 metabolites within MSC-treated ALI and PBS-treated ALI at three time points are potential biomarkers for immune modulation after MSC treatment (Supplementary Table S3A-B).

From another perspective, certain metabolites or pathways may not serve as biomarkers but powerful mediators for immune responses. We believe that under the influence of MSCs, liver-resident immune cells break their commitment to particular metabolic fate. Different immunologic outcomes can be achieved by interfering with these metabolites and pathways as they are in charge of immune functions. Using pathway analysis, we identify 3 metabolic pathways that are significantly regulated in PBS-treated ALI versus the sham group, and assume that they play a crucial role in providing energy and intermediates for ALI-activated immunity. 13 pathways exhibit a significant variation between MSC-treated ALI and PBS-treated ALI, with $p\text{-}value < 0.05$, for instance, aminoacyl-tRNA biosynthesis; this can be interpreted as an underlying mechanism of MSC-orchestrated immune modulation, where gene translation is regulated by the availability of certain amino acids in an anti-inflammatory pattern, leading to improved homeostasis and ALI prognosis.

The overlap of certain metabolites and pathways in both cases sheds an intriguing light on the association between MSC-modulated immune metabolism and ALI remission. In this work, arginine, glutamate and aspartate metabolism are found to be most affected in both cases. We speculate that these three pathways are fundamental for ALI-activated immunity, and the perturbation of them may account for MSC-ameliorated ALI. This hypothesis can be supported by the interplay between immunity and metabolism that has been demonstrated in detail from the previous work.

To begin with, arginine metabolism generates nitric oxide (NO) by nitric oxide synthase (NOS) as an important toxic defense molecule. NO synthesis in macrophages and neutrophils has been proved to be an essential mechanism against pathogen, in which iron-sulfur-containing proteins in the electron transport chain are dysfunctioned via NO nitrosylation, leading to mitochondrial collapse. In the case of ALI, NO and its derivative, peroxynitrite, may be deleterious for liver regeneration as they have the ability to oxidase proteins, amino acids, lipids, and DNA, accelerating cell injury and death. Arginase (ARG) competes against NOS for arginine to form ornithine and urea [24]; activation of ARG1 has been proposed as a hallmark for “alternatively activated macrophages” [25] that promote the resolution of inflammation and tissue repair. In our work, a decreased level of citrulline and an increased level of ornithine is detected in PBS-treated ALI compared to MSC-treated ALI (Fig. 3D), indicating that provision of MSCs may help immune cells shunt arginine into ARG1 hydrolysis, and as a result moderate immune responses and ALI severity.

Glutamate and aspartate metabolism plays indispensable roles in regulating immune cell proliferation, growth, cytotoxic activities, and energy regeneration [26]. Aspartate and glutamate metabolism generates precursors for purine and pyrimidine nucleotides that are essential for lymphocytes proliferation. Aspartate, glutamate and glutamine can act as major energy substrate for various immune responses. Glutamine and glutamate are crucial for glutathione biosynthesis, and subsequently relieve oxidative stress after CCl_4 administration.

Notably, as distinct metabolic pathways diverge and converge at many levels [27], alterations of these three pathways should not be viewed individually but integratedly. For instance, glutamine is extensively converted into primarily glutamate via glutaminolysis, and to a lesser extent, aspartate, which is required for recycling citrulline and sustaining NO production. In this way, arginine, glutamate and aspartate metabolism interact with one another during metabolic shifts. After taking a closer look at pathway analyses, we pick out eight metabolites that are significantly regulated in both cases (Fig. 3D) as joints for the network of arginine, aspartate and glutamate metabolism (Fig. 4). These metabolites and pathways may help construct a metabolic cascade during immune modulation, as they transmit and amplify perturbations in one pathway to another. The inspiration is that exogenous supply of certain metabolite may have a profound impact on the metabolic network, crosstalking with immune responses and modulating its outcomes in ALI rescue.

Even though the roles of these key metabolites and signaling pathways were not validated in this study, we believe that our results will eventually facilitate the understanding of the interplay between MSCs and liver-resident immune cells during ALI. The featured metabolomic profiles detected in this study imply altered status of liver-resident immune cells, which provide further support for the idea from previous studies that MSCs play an immune regulatory role during ALI rescue. Future investigations should be made in large studies to decipher the physiological roles of these metabolites and their upstream/downstream interactions.

5. Conclusions

Using a newly developed CIL LC-MS metabolomic platform, we discovered a large number of metabolites that are statistically significant within MSC-treated ALI and PBS-treated ALI groups. PCA and OPLS-DA analyses reveal featured metabolomic profiles of the liver-resident immune cells in PBS-treated ALI, MSC-treated ALI and the sham group. 4295 peak pairs are quantified and 2461 are further identified in zero-reaction and one-reaction libraries. 256 metabolites are identified to be candidate biomarkers for ALI-activated immunity and 114 metabolites are identified to be candidate biomarkers for MSC-modulated immunity. Using pathway analysis, ariginine, aspartate and glutamate metabolism are found to be most affected in both cases, with eight significantly regulated metabolites (glutamic-gamma-semialdehyde, aspartate acid, glutamate acid, gamma-Aminobutyric acid-orinithine, 2-keto-glutaramic acid, *N*-acetylornithine, citrulline and ornithine) serving as joints. We also speculate that these metabolites and pathways are not biomarkers but powerful mediators for immune responses, as they play a crucial role in immune cell proliferation, providing energy, intermediates and host defense molecules for cytotoxic activities. The potential immune regulatory role of certain metabolite needs to be further investigated and will be of great therapeutic

value for ALI rescue, as they may help construct a metabolic cascade during immune modulation, transmitting and amplifying perturbations in one pathway to another and subsquently achieving different immunologic outcomes.

Conflicts of interest

No competing financial interests exist regarding the subject matter or materials discussed in the presented work.

Author contributions

S.Z: conception and design; X.S and J.Y: cell preparation and ALI model; J.L, H.X and L.Z: immunohistochemical detection and the cell proliferation assay; X.S, D.C, and M.Z: analyzed and interpreted the data; X.S and D.C: drafted the manuscript; L.L: technical support; L.L and S.Z supervised the study.

Acknowledgments

We thank Dr. Yanyuan Li for providing technical support for pathology and also thank Dr. Wei Han for his assistance with metabolomics methodology. This work is supported by Innovative Research Groups of National Natural Science Foundation of China (No. 81721091).

Appendix A. Supplementary data

Supplementary data to this article can be found online at https://doi.org/10.1016/j.yexcr.2019.111511.

References

[1] W. Bernal, G. Auzinger, A. Dhawan, et al., Acute liver failure 369 (2013) 2525–2534.
[2] L.L. Kjaergard, L. Jianping, A.N. Bodil, et al., Artificial and bioartificial support systems for acute and acute-on-chronic liver failure, a systematic review 289 (2003) 217–222.
[3] M.E. Guicciardi, Apoptosis: a mechanism of acute and chronic liver injury, Gut 54 (2005) 1024–1033.
[4] Z. Wu, M. Han, T. Chen, et al., Acute liver failure: mechanisms of immune-mediated liver injury, Liver Int. 30 (2010) 782–794.
[5] T.K. Kuo, S.P. Hung, C.H. Chuang, et al., Stem cell therapy for liver disease: parameters governing the success of using bone marrow mesenchymal stem cells, Gastroenterology 134 (2008) 2111–2121 2121 e2111-2113.
[6] K. Le Blanc, D. Mougiakakos, Multipotent mesenchymal stromal cells and the innate immune system, Nat. Rev. Immunol. 12 (2012) 383–396.
[7] Y.J. Chang, J.W. Liu, P.C. Lin, et al., Mesenchymal stem cells facilitate recovery from chemically induced liver damage and decrease liver fibrosis, Life Sci. 85 (2009) 517–525.
[8] L. Deng, G. Liu, X. Wu, et al., Adipose derived mesenchymal stem cells efficiently rescue carbon tetrachloride-induced acute liver failure in mouse, ScientificWorldJournal 2014 (2014) 103643.
[9] P. Semedo, M. Correa-Costa, M. Antonio Cenedeze, et al., Mesenchymal stem cells attenuate renal fibrosis through immune modulation and remodeling properties in a rat remnant kidney model, Stem Cells 27 (2009) 3063–3073.
[10] R. Wang-Sattler, Z. Yu, C. Herder, et al., Novel biomarkers for pre-diabetes identified by metabolomics, Mol. Syst. Biol. 8 (2012) 615.
[11] A.F. McGettrick, L.A.J. O'Neill, How metabolism generates signals during innate immunity and inflammation, J. Biol. Chem. 288 (2013) 22893–22898.
[12] S. Zhao, M. Dawe, K. Guo, et al., Development of High-Performance Chemical Isotope Labeling LC-MS for Profiling the Carbonyl Submetabolome vol. 89, (2017) acs.analchem.7b01098.
[13] H. Zhu, Z.K. Guo, X.X. Jiang, et al., A protocol for isolation and culture of mesenchymal stem cells from mouse compact bone, Nat. Protoc. 5 (2010) 550–560.
[14] C.F.B. Matthew A. Lorenz, Robert T. Kennedy, Reducing Time and Increasing Sensitivity in Sample Preparation for Adherent Mammalian Cell Metabolomics. .
[15] X. Luo, S. Zhao, T. Huan, et al., High-performance chemical isotope labeling liquid chromatography-mass spectrometry for profiling the metabolomic reprogramming elicited by ammonium limitation in yeast, J. Proteome Res. 15 (2016) 1602–1612.
[16] G.L. Backes, D.M. Neumann, B.S. Jursic, Synthesis and antifungal activity of substituted salicylaldehyde hydrazones, hydrazides and sulfohydrazides, Bioorg. Med. Chem. 22 (2014) 4629–4636.
[17] M.A. Lorenz, C.F. Burant, R.T. Kennedy, J Analytical Chemistry, Reducing time and increasing sensitivity in sample preparation for adherent mammalian cell metabolomics 83 (2011) 3406.
[18] G. Kevin, L.J.A.C. Liang, Differential 12C-/13C-isotope dansylation labeling and fast liquid chromatography/mass spectrometry for absolute and relative, quantification of the metabolome 81 (2009) 3919–3932.
[19] R. Zhou, C.L. Tseng, T. Huan, et al., IsoMS: automated processing of LC-MS data generated by a chemical isotope labeling metabolomics platform, Anal. Chem. 86 (2014) 4675–4679.
[20] T. Huan, L. Li, Counting missing values in a metabolite-intensity data set for measuring the analytical performance of a metabolomics platform, Anal. Chem. 87 (2015) 1306–1313.
[21] T. Huan, L. Li, Quantitative metabolome analysis based on chromatographic peak reconstruction in chemical isotope labeling liquid chromatography mass spectrometry, Anal. Chem. 87 (2015) 7011–7016.
[22] L. Li, R. Li, J. Zhou, et al., MyCompoundID: using an evidence-based metabolome library for metabolite identification, Anal. Chem. 85 (2013) 3401–3408.
[23] T. Squillaro, G. Peluso, U. Galderisi, Clinical trials with mesenchymal stem cells: an update, Cell Transplant. 25 (2016) 829–848.
[24] C. Bogdan, Nitric oxide and the immune response, Nat. Immunol. 2 (2001) 907–916.
[25] F.O. Martinez, L. Helming, S. Gordon, Alternative activation of macrophages: an immunologic functional perspective, Annu. Rev. Immunol. 27 (2009) 451–483.
[26] P. Li, Y.-L. Yin, D. Li, et al., Amino acids and immune function, Br. J. Nutr. 98 (2007).
[27] Erika L. Pearce, Edward J. Pearce, Metabolic pathways in immune cell activation and quiescence, Immunity 38 (2013) 633–643.